Article



Allosteric Effects of the Proton Donor on the Microbial Proton Pump Proteorhodopsin

Sadegh Faramarzi, ¹ Jun Feng, ¹ and Blake Mertz^{1,*}

¹C. Eugene Department of Chemistry, West Virginia University, Morgantown, West Virginia

ABSTRACT Proteorhodopsin (PR) is a microbial proton pump that is ubiquitous in marine environments and may play an important role in the oceanic carbon cycle. Photoisomerization of the retinal chromophore in PR leads to a series of proton transfers between specific acidic amino acid residues and the Schiff base of retinal, culminating in a proton motive force to facilitate ATP synthesis. The proton donor in a similar retinal protein, bacteriorhodopsin, acts as a latch to allow the influx of bulk water. However, it is unclear if the proton donor in PR, E108, utilizes the same latch mechanism to become internally hydrated. Here, we used molecular dynamics simulations to model the changes in internal hydration of the blue variant of PR during photoactivation with the proton donor in protonated and deprotonated states. We find that there is a stark contrast in the levels of internal hydration of the cytoplasmic half of PR based on the protonation state of E108. Instead of a latch mechanism, deprotonation of E108 acts as a gate, taking advantage of a nearby polar residue (S61) to promote the formation of a stable water wire from bulk cytoplasm to the retinal-binding pocket over hundreds of nanoseconds. No large-scale conformational changes occur in PR over the microsecond timescale. This subtle yet clear difference in the effect of deprotonation of the proton donor in PR may help explain why the photointermediates that involve the proton donor (i.e., M and N states) have timescales that are orders of magnitude different from the archaeal proton pump, bacteriorhodopsin. In general, our study highlights the importance of understanding how structural fluctuations lead to differences in the way that retinal proteins accomplish the same task.

INTRODUCTION

Proteorhodopsin (PR) is a microbial proton pump that was first identified in marine phytoplankton (1), and its discovery spawned the field of metagenomics. Two variants of PR exist (green PR (GPR) and blue PR (BPR) (2)) that have adapted to optimize the depth-dependent wavelengths of light at which they reside in the ocean. Since their initial discovery, PR-encoding genes have also been found in freshwater bacteria (3), soil-bound bacteria (4), viruses (5), and eukaryotes (6). Although the exact biological role of PR is undetermined, it may be a vital component in several marine ecosystems, notably the carbon cycle for degradation of complex organic matter (7) and as a secondary source of ATP synthesis in iron-deficient regions of the ocean (8). In addition, PR has the potential for applications in solar-to-chemical energy conversion (9).

PR is a member of the microbial retinal protein family, proteins with a seven-transmembrane α -helical topology and a retinal chromophore that is covalently bound to a lysine residue on helix G. Absorption of a photon of light

Submitted May 10, 2018, and accepted for publication August 22, 2018.

*Correspondence: blake.mertz@mail.wvu.edu

Editor: Anatoly Kolomeisky.

https://doi.org/10.1016/j.bpj.2018.08.028

© 2018 Biophysical Society.

leads to an all-trans to 13-cis isomerization, initiating the photocycle (10). This structural rearrangement of the retinal-binding pocket leads to a shift in the pK_a of key acidic residues in the interior of PR that allows for proton transfers to take place (the proton acceptor (D97), proton donor (E108), and proton release group (as yet unidentified)) (11) (Figs. 1 and S1). Each proton transfer is characterized by a spectroscopically distinct photointermediate, with the end product being a net transport of one proton across the inner membrane to the periplasmic space of the bacterial cell. This proton gradient can then be used for synthesis of ATP.

The majority of what we know about microbial proton pumps comes from decades of research on bacteriorhodopsin (bR) (12–14). Although many similarities exist between bR and PR, PR possesses several unique characteristics that must be elucidated to fully understand how it generates a proton motive force. The timescales for the first half of the photocycle of GPR are noticeably faster than that of bR (14,15), even though the complete photocycle of PR is an order of magnitude slower (16). In addition, the pK_a of the proton acceptor is noticeably higher (7.1–7.6 (10,17)) than bR (2.6 (18)), leading to an ability for PR to invert the direction of proton pumping at a low pH (19). In bR,



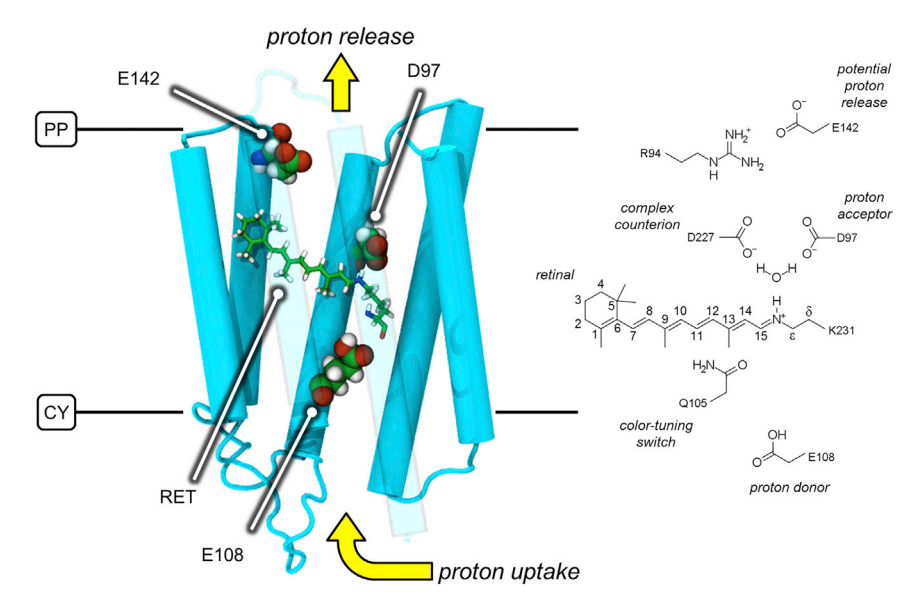


FIGURE 1 PR functions as a proton pump. The tertiary structure of BPR (PDB: 4JQ6) is located on the left. The chemical structure of retinal and important residues in the photocycle of PR is located on the right. Upon photoisomerization of retinal (RET), PR proceeds through its photocycle, utilizing a series of proton transfers to facilitate proton pumping. The initial proton transfer occurs from the protonated Schiff base (PSB) to the proton acceptor, D97. The Schiff base then becomes reprotonated by the proton donor, E108. E108 is then protonated from bulk cytoplasm, and D97 donates its proton to the putative proton release group, E142, allowing an excess proton to be released in the the periplasmic space. CY, cytoplasmic side of the inner membrane; PP, periplasmic side of the inner membrane. To see this figure in color, go online.

the proton release group is composed of a pair of glutamic acids (20), but in PR there is a lack of corresponding residues. Finally, a single residue in the retinal-binding pocket at position 105 (a leucine in GPR and a glutamine in BPR) acts as a color-tuning switch between the two variants of PR (21).

The cytoplasmic half of both bR and PR undergo largescale conformational changes that allow for an influx of bulk water in the later stages of their respective photocycles (14). This influx is necessary to form a stable water wire to bridge the 10- to 15-Å gap that exists between the proton donor and the protonated Schiff base (PSB) of retinal and allow for proton transfer through a Grotthuss mechanism (22–25). In bR, the proton donor controls the outward movement of helices E, F, and G; deprotonation of this residue leads to the opening of the protein on the nanosecond timescale (26). This rapid release of the helical bundle in bR (i.e., "latch mechanism") has a twofold purpose: 1) to form the water wire and 2) to prevent backflow of protons that impede the photocycle (27). Although PR has a glutamic acid (E108) in the same position as the proton donor in bR, it lacks a pair of glutamic acids that act as a proton uptake complex (28) as well as a hydrogen-bonding partner in helix B that lies directly across from the proton donor (12). In addition, an acidic residue as the proton donor is not conserved among other PR-like proton pumps, such as a lysine in Elasmotherium sibiricum rhodopsin (29) and a histidine on helix B in eubacterial proton pumps (30). Our recent computational study of PR hinted that the protonation state of the proton donor in PR may have a more subtle influence on the internal hydration of protein because we did not observe the latch mechanism seen in bR (31).

In this work, we set out to characterize the effect of protonation of the proton donor in blue PR, E108, on the early photointermediates of the PR photocycle using molecular dynamics (MD) simulations. The most well validated structure of PR is from the blue variant in the dark state (32), limiting us to a microsecond-timescale investigation of the dark and K states. (Deprotonation of E108 normally occurs during the formation of the N photointermediate in the photocycle). We find that deprotonation of E108 controls the interior hydration of the cytoplasmic half of PR, with full hydration occurring over hundreds of nanoseconds. Unlike in bR, there is no large-scale conformational change associated with deprotonation of the proton donor; rather, E108 acts as a gate that opens and closes to allow or deny access to the internal water channel. In addition, we observe a significant degree of cross talk between E108 and the colortuning switch in PR as well as differences in interactions of the retinal-binding pocket that may help explain how proton release occurs in PR.

METHODS

Equilibrium MD

The x-ray crystal structure of BPR from Med12 in the dark state (Protein Data Bank (PDB): 4JQ6) (32) was used as the starting structure. Missing loops were modeled based on the loops of the NMR structure of GPR (PDB: 2L6X) (33). We have truncated the N- and C-termini (D9 to S231 are included) and have numbered residues based on GPR.

Two sets of equilibrium MD simulations were carried out based on the protonation state of E108. In the protonated state, the $O_{\delta 2}$ oxygen of the carboxylic group is protonated, and in the deprotonated state, both oxygens of the carboxylic terminal group are deprotonated. In the protonated state of E108, partial charges of the terminal OE1, OE2, and HE2 atoms are -0.55, -0.61, and 0.44, respectively. The carboxylic OE1 and OE2 atoms in the deprotonated state of E108 have equal partial charges of -0.76. The ionization states of all other residues are identical between the two sets of simulations. Based on our earlier simulations of PR (31), we protonated H75 on the N_{δ} atom of the imidazole ring. The putative proton release group, E142, is deprotonated because its pK_a is reported to be < 7.5 in BPR (34).

PR with protonated E108 was placed within 160 lipid molecules (80 per leaflet) with a molar ratio of 3:1 1-palmitoyl-2-oleoyl-sn-glycero-3-phosphoethanolamine/1-palmitoyl-2-oleoyl-sn-glycero-3-phosphoglycerol as a proxy for a gram-negative inner membrane (35) using the replacement method (36,37) of the CHARMM-GUI server (http://www.charmm-gui. com) (38,39). After solvation with 7867 water molecules (transferable intermolecular potential with three points) and ionization with 44 sodium ions (to neutralize the system), the total system size was 47,288 atoms. The corresponding system with deprotonated E108 has 129 lipids (65 and 64 in upper and lower leaflets, respectively) with the same 3:1 molar ratio of 1-palmitoyl-2-oleoyl-sn-glycero-3-phosphoethanolamine/1-palmitoyl-2oleoyl-sn-glycero-3-phosphoglycerol. There were 7030 water molecules, 38 sodium ions, and 1 chloride ion for a total of 40,880 atoms.

The systems were minimized and equilibrated with NAMD 2.10 (40) based on the CHARMM-GUI protocol with the CHARMM c36 force field for lipids and proteins (41). The minimization and equilibration protocol involves six steps that gradually remove restraints from the protein backbone, lipids, water molecules, and ions over 375 ps (36). Retinal force field parameters were obtained from Scott Feller (42,43). After equilibration, the systems and force fields were converted to formats compatible with Assisted Model Building with Energy Refinement (AMBER) in CHAMBER (44), and all production simulations were run with AMBER 12 and AMBER 16 packages with graphics processing unit acceleration (45,46). All equilibrium MD simulations were run in the NPT ensemble at 300 K and 1 bar using a Langevin thermostat and a Berendsen barostat (relaxation time of 8 ps) with a 2 fs timestep. A cutoff of 8 Å was applied for nonbonded interactions. To initiate K-state simulations through all-trans to 13-cis isomerization of retinal, the torsional potential of the C13=C14 bond was temporarily lowered, as has been done previously for PR (31) and rhodopsin (47).

Thermodynamic integration

Thermodynamic integration (TI) is a technique that determines the free energy associated with an alchemical transformation between two states (48,49), defined as

$$\Delta A = \int_0^1 \left\langle \frac{\delta H(x, \rho_x; \lambda)}{\delta \lambda} \right\rangle_{\lambda} d\lambda, \tag{1}$$

where H is the Hamiltonian of the system and λ is the coupling parameter that represents the transition from deprotonated ($\lambda = 0$) to protonated ($\lambda = 1$) in E108. The parameters x and ρ_x are the coordinate and momentum, respectively. Snapshots were taken from dark-state equilibrium MD simulations with E108 protonated as starting coordinates for TI calculations. A dual topology was assigned to E108, one for each protonation state. Initial TI simulations were run at 16 λ values equally spaced between 0 and 1. Follow-up TI simulations were carried out from $\lambda = 0.0$ to 0.1 at 0.02 intervals to avoid overestimates of $\langle \frac{\delta U}{\delta \lambda} \rangle$ as λ approaches zero. A soft-core potential was also used to avoid end-point catastrophes at $\lambda = 0$ and 1. TI simulations were run in NAMD 2.12 (40) in the NVT ensemble with T = 310 K and with a 0.5 fs timestep for 20 ns for each λ value. A cutoff of 12 Å with force-switching at 10 Å was applied for nonbonded interactions. The trapezoidal rule was used to calculate the free energy of transformation, which was subsequently used to obtain the pK_a of E108.

Analysis

Visual MD (50) was used for analysis of angles, interatomic distances, solvent accessibility, hydrogen bonds, and root mean-squared deviation. Images of representative snapshots were rendered in either visual MD or PyMOL (51). Water density maps were calculated with MDAnalysis (52). CAVER 3.0 (53,54) was applied to each trajectory every 4 ns to detect cavities inside PR that could allow diffusion of water. The probe radius was 0.8 Å, with a shell radius of 3 Å and a shell depth of 4 Å. A threshold of 10 was used for clustering tunnels. For hydrogen bond analysis, a distance threshold of 3 Å and an angle threshold of 20° was used (where the angle is defined by the vectors of 1) the heavy atom of the hydrogen bond donor and the hydrogen of the hydrogen bond donor and 2) the heavy atom of the hydrogen bond acceptor and the hydrogen of the hydrogen bond donor). N-body information theory was used to identify the correlation of dynamics between distant residues. The methodology uses configurational entropy of molecules in MD trajectories to identify distal residues that communicate with each other or organize dynamics within functional sites (55,56).

RESULTS AND DISCUSSION

Deprotonation of E108 leads to an increase in hydration from bulk cytoplasm

A detailed examination of the proton donor, E108, reveals that titration of the side chain has a very specific purpose: to prohibit internal hydration and subsequent interaction with the PSB. At the most fundamental level, this function manifests itself in the orientation of the E108 side chain. In the dark state, the χ_1 dihedral has a dominant conformation at -70° , regardless of protonation state. However, the χ_2 dihedral is highly dependent on protonation state of E108: when protonated, χ_2 predominantly has a $\pm 180^{\circ}$ orientation, leading to a linear conformation that occludes the interior channel of the cytoplasmic half of PR from bulk cytoplasm (Figs. 2 A, S2, and S3). In contrast, when E108 is deprotonated, the χ_2 dihedral is -65° , corresponding to an outward rotation toward bulk cytoplasm. (We would emphasize that although our simulations are well beyond the timescale for the dark-state → K-state transition (picoseconds), the effects of deprotonation of E108 reported here occurred in a majority but not all of our trajectories. Further discussion can be found in the Supporting Material.)

Upon isomerization of retinal and the transition to the K state, the side-chain orientation when E108 is deprotonated is largely unaffected. In contrast, when E108 is protonated, both the χ_1 and χ_2 dihedral angles shift to a bimodal distribution, with a loss of sampling in the region of -70° , 60° (χ_1, χ_2) (Fig. 2 B). The corresponding rearrangement of the sampling landscape of the E108 side chain in the protonated state indicates that the side chain prefers to be in a completely linear orientation. This indicates that there is a degree of coupling existing between E108 and retinal that will be discussed below. In addition, we can further characterize the hydration of the side chain of E108 by calculating its solvent-accessible surface area (SASA). It appears that a dihedral orientation of $\pm 180^{\circ}$ at either of the χ dihedrals is sufficient to prevent the interior channel of PR from becoming hydrated: in both the dark and K states, the SASA of the side chain of E108 when protonated is less than 10 Å² (i.e., essentially dehydrated) (Fig. S4). In contrast, the SASA of E108 when it is deprotonated fluctuates from 20 to 80 Å² (Fig. S4).

When expanding the scope of analysis beyond E108, we see that the protonation state of E108 also has a marked

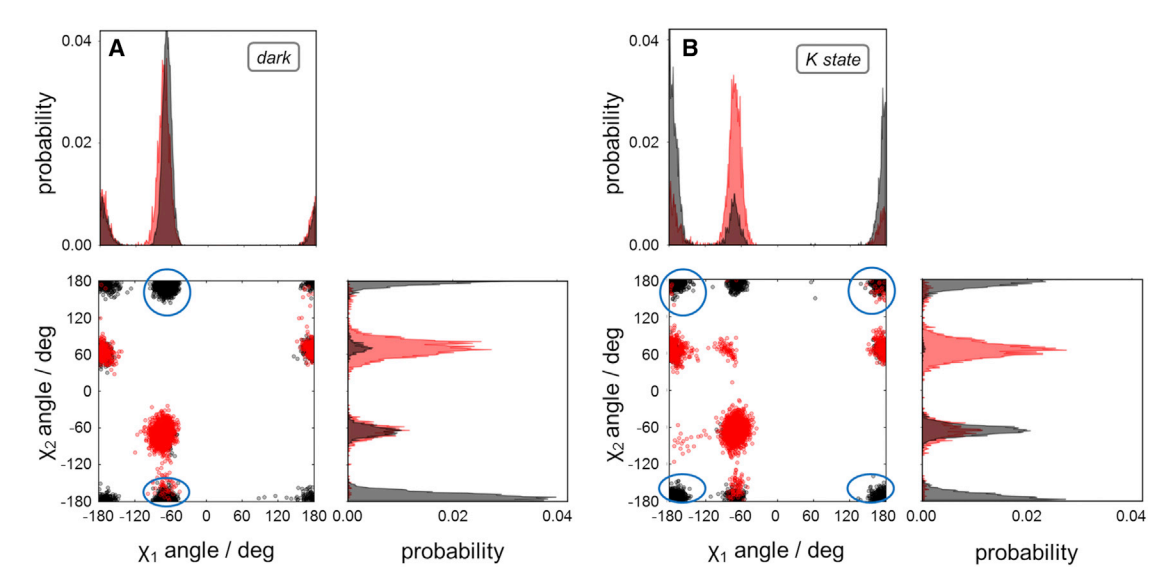


FIGURE 2 Protonation state of E108 strongly influences its side chain-orientation. (A) Normalized histograms of the χ_1 and χ_2 dihedral angles of E108 in the dark state are shown. When E108 is protonated (black), the dominant orientation of the χ_2 dihedral is $\pm 180^{\circ}$, leading to a fully extended side chain and blockage of the interior channel from the cytoplasmic end of PR to the retinal-binding pocket. When E108 is deprotonated (red), the dominant χ_2 dihedral is -65°, i.e., allowing the side chain to be oriented away from the retinal-binding pocket and opening the cytoplasmic half channel inside the protein for hydration from bulk solvent. Unlike χ_2 , the dominant orientation of the χ_1 dihedral for E108 in both protonated (black) and deprotonated (red) states is -60° , leading to the conclusion that the χ_2 dihedral angle is the determining factor in side-chain orientation of E108 in the dark state. (B) Normalized histograms of the χ_1 and χ_2 dihedral angles of E108 for PR in the K state are shown. No noticeable changes occur for the side-chain orientation of the deprotonated state of E108 for both χ_1 and χ_2 (red). However, the bimodal distribution of the χ_1 and χ_2 side-chain orientation of E108 between closed and open conformations when protonated (black) undergoes a shift; χ_2 becomes more evenly distributed, whereas χ_1 shifts toward $\pm 180^\circ$, leading to transient access of bulk waters to the interior of the protein. Circles highlight the shift of the χ_1 and χ_2 side-chain orientation from the dark to the K state when E108 is protonated. deg, degree. To see this figure in color, go online.

effect on its interactions with a polar residue in helix B, S61 (Table 1). In the protonated state, the side chain of E108 is much less likely to lie within a range in which it is possible to form a hydrogen bond with S61. However, upon deprotonation, the distance between the side chains of E108 and S61 becomes noticeably smaller (1-3 Å), to the point at which a stable hydrogen bond is formed on the microsecond timescale (Figs. 3 A and S5). Inspection of the cytoplasmic half of PR shows that the hydrogen bond between E108 and S61 is essential to facilitate interior hydration of the cytoplasmic half of the protein (Fig. 3 B). When E108 is protonated, the side chain of the residue is oriented toward the PSB, occluding the proximal space of the binding pocket and preventing formation of a coordinated system of water molecules. In contrast, when E108 is deprotonated, the hydrogen bond formed with S61 provides a stable checkpoint for intercalated waters to diffuse into and out of the interior channel, connecting the retinal-binding pocket with bulk cytoplasmic solvent. This result is consistent with our previous study

TABLE 1 Fraction of Time a Hydrogen Bond Forms between E108 and S61 in PR

System	Dark State	K State	
Protonated	0.18	0.20	
Deprotonated	0.55	0.40	

(31) and is also conserved in other retinal proteins closely related to PR: in E. sibiricum rhodopsin, this residue is a threonine, and in xanthorhodopsin and the sodium pump KR2, it is a serine. Most notably in bR, the proton donor, D96, forms a hydrogen bond with T46. In crystal structures of bR in the dark and N states, this hydrogen bond rearranges to accommodate an influx of waters from the cytoplasm (12,57). Specifically, D96 recruits waters from bulk cytoplasm, and in the progression toward the N photointermediate, the interaction of the T46 and D96 side chains provides a key stabilizing force for a water molecule to diffuse between the two. The unique aspect of the conserved behavior between PR and bR with respect to this hydrogen bond is that S61 lies 1.5 turns farther away from the interior of PR on helix B: the side chain of E108 is predisposed to have a χ_2 dihedral that favors an orientation that facilitates the formation of the hydrogen bond (Fig. S5).

A marked contrast from bR in our simulations is that there is no large-scale conformational change in the cytoplasmic side of the protein upon deprotonation of E108. MD simulations of the different photointermediate states of bR, with the proton donor either protonated or deprotonated, showed that deprotonation of the proton donor led to a rapid opening of the cytoplasmic side of the protein (26) (i.e., within 50 ns). It was hypothesized that the proton donor serves as a "latch," with deprotonation triggering the release of this

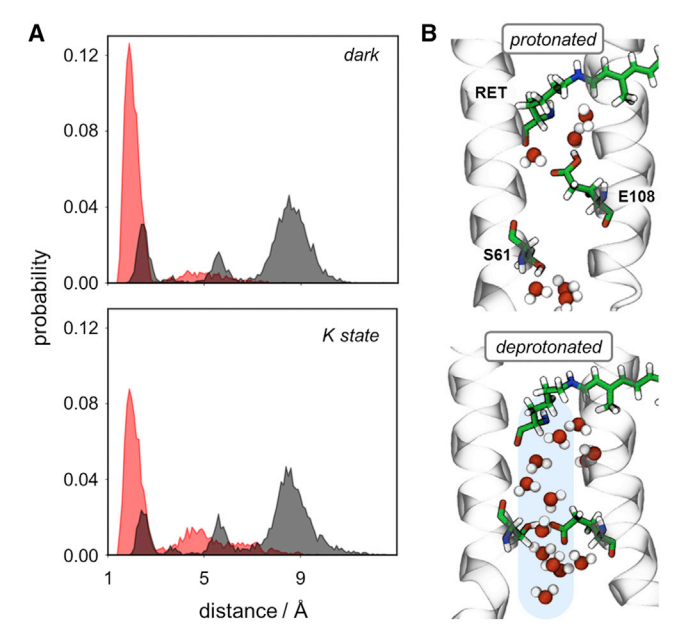


FIGURE 3 E108 shows a noticeably higher propensity to form a hydrogen bond with S61 in the deprotonated state. (A) A histogram of the distance between the center of mass of the two terminal oxygens of E108 and the hydrogen of S61 is shown. When E108 is deprotonated (red), the side chain of the acidic residue is in much closer proximity to the side chain of S61, facilitating the formation of a hydrogen bond. In contrast, when E108 is protonated (black), the distance between the side chains of E108 and S61 is usually too large to form a direct hydrogen bond. This relationship stays consistent for both the dark (top) and K (bottom) states. (B) Representative snapshots of the cytoplasmic interior of PR when E108 is in the protonated (top) and deprotonated (bottom) states are shown. Sticks indicate the residues involved in the interaction of waters from bulk cytoplasm to the retinal (RET)-binding pocket, spheres indicate the water molecules, and ribbons indicate helices B (left) and C (right) of PR. To see this figure in color, go online.

latch. A subsequent study on a triple mutant of bR in which the dark-state conformation had an open cytoplasmic end showed that this fast response of the latching mechanism may play a vital role in preventing backflow of protons into bulk cytoplasm (27). More recently, it was revealed that proton uptake in bR utilizes a cluster of residues to stabilize interactions of the proton donor with bulk cytoplasmic waters, leading to modulation of the later stages in the photocycle (28). PR does not possess a corresponding aspartic acid residue, so it would make sense that the proton donor behaves differently from bR. Based on our simulations of PR in the dark and K states, it appears that the protonation-dependent orientation of E108 is sufficient to control passage of waters into the cytoplasmic half channel of PR. We do not observe any major conformational fluctuations of the protein based on root mean-squared fluctuations (Fig. S6).

To further characterize the local environment around E108, we carried out TI calculations. The pK_a of E108 when PR is in the dark state based on these calculations is 10.3. No pK_a of E108 in BPR has been determined experimentally; studies on GPR have determined that the pK_a of E108 is at least >8.5 (19) or that it is similar to the proton donor in bR (>11) (10). This p K_a is well above the pH of marine environments (around 7.6), meaning that E108 would remain protonated in the dark state. Deprotonation of E108 would presumably occur when the local environment undergoes rearrangement to expose the residue to bulk water, i.e., during the outward tilt of helices F and G that is characteristic of the $M \rightarrow N$ transition. Our TI calculations are consistent with what is known about proton donors in retinal proteins; because the cytoplasmic side of PR in our simulations has not opened, the area around E108 has yet to shift from a hydrophobic to a hydrophilic environment. This shift is a prerequisite for decreasing the pK_a of the proton donor to facilitate proton transfer from E108 to the Schiff base. These calculations also help emphasize how PR is markedly different from bR with respect to the proton donor, as deprotonation of the proton donor led to large-scale conformational changes in bR regardless of the photointermediate that was used as a starting structure (26). The presence of a proton switch on the third transmembrane helix is also important in several class A G-protein-coupled receptors; in rhodopsin, E134 is part of an ionic lock that releases the cytoplasmic half of the protein to allow for reprotonation of the Schiff base and activation of the G-protein, transducin (58,59).

Long-range effects of the protonation of E108 on hydration in PR

Inspection of the entire protein reveals that the protonation state of E108 has long-range effects as well. In most retinal proteins, the cytoplasmic half channel between the proton donor and the Schiff base undergoes subtle rearrangements immediately after photoactivation. It is only in the later stages of the photocycle (N and O states) that large-scale conformational changes in the cytoplasmic side of PR take place (14). This lack of large changes within the protein is also the case in our simulations. For both protonation states of E108, the distance between the side chain of E108 and the PSB remains fairly stable in both the dark and K states (Fig. 4 A). It appears that the side-chain orientation of E108 is the major determining factor in internal hydration of the cytoplasmic half channel; when E108 is protonated, 1–2 water molecules diffuse into the channel, whereas when E108 is deprotonated, we observe an influx of water (up to 10 water molecules in the K state) (Fig. 4 B). Interestingly, this increase in hydration for the deprotonated form of E108 is not restricted to the cytoplasmic half of PR. The periplasmic half of PR remains largely dehydrated in the dark state and with E108 protonated; when E108 is deprotonated, 2-3 times as many waters diffuse into the protein (Fig. 4 C). After isomerization of retinal, the levels of hydration between the protonation states of

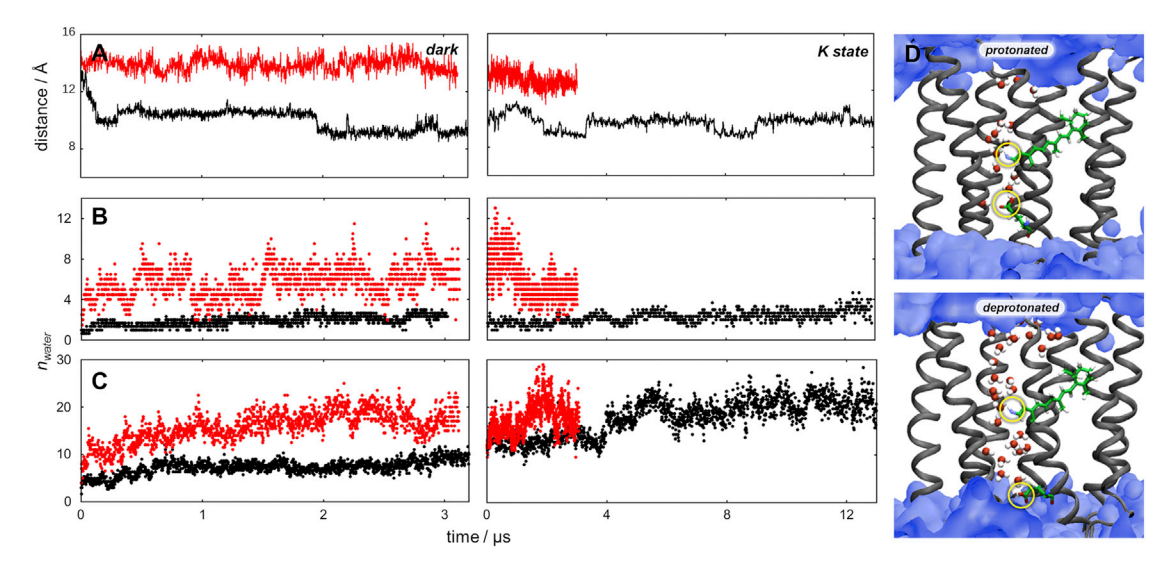


FIGURE 4 Deprotonation of E108 has proximal and distal effects on the hydration of BPR. (A) The distance between the PSB and carboxylate side chain of E108 in the deprotonated (red) versus the protonated (black) states in the dark (left) and K (right) states is shown. Simulations with E108 in the deprotonated state have a much larger separation in the cytoplasmic half channel, because of how the orientation of the E108 side chain is away from the retinalbinding pocket. (B) The number of water molecules in the cytoplasmic half-channel of PR, defined as the region inside PR between the nitrogen of the Schiff base and the carboxylic oxygen of E108. The number of waters when E108 is deprotonated (red) steadily increases in the dark state (left), whereas the cytoplasmic half channel stays dehydrated when E108 is protonated (black). In the K state (right), hydration fluctuates more but remains around four waters when E108 is deprotonated, whereas when E108 is protonated, the protein remains dehydrated. (C) The number of water molecules in the periplasmic (PP) halfchannel of PR, defined as the region inside PR between the nitrogen of the Schiff base and the carboxylic carbon of E142. In the dark state (left), both titration states of E108 lead to an increase in internal hydration, with a more noticeable increase when E108 is deprotonated (red). In the K state (right), the number of waters fluctuates but remains at about 20 water molecules with E108 in the deprotonated state. When E108 is protonated (black), hydration increases after isomerization of retinal, stabilizing around 20 waters. (D) Representative snapshots of PR with E108 protonated (top) or deprotonated (bottom) are shown. The surface indicates bulk water; ribbons indicate the backbone of PR, sticks indicate the retinal, and spheres indicate individual internal water molecules. Schiff base and E108 side chains are highlighted for clarity. To see this figure in color, go online.

E108 becomes indistinguishable. This behavior indicates that E108 may be subtly influencing the retinal-binding pocket, as will be discussed in more detail below.

If we look at the average water density of the interior of the protein for both protonation states of E108 in the dark and K states, a clearer picture of the mechanism of proton pumping emerges. When E108 is deprotonated, two stable half channels of water, connected by retinal, form from the cytoplasmic to the periplasmic side of the protein (Fig. S7). This continuous water channel exists regardless of the dark or K state. In contrast, when E108 is protonated, only the periplasmic half channel becomes hydrated and only in the K state. If we analyze the formation of these half channels, identifying potential half channels that exist at a given frame in our trajectories, we observe similar behavior. A significantly larger number of pathways exist in the cytoplasmic side of PR when E108 is deprotonated, whereas few pathways exist when E108 is protonated. In the periplasmic half of PR, a large number of pathways exist in both photointermediates when E108 is deprotonated, and when E108 is protonated, a transition from few to many pathways occurs from the dark to the K state (Fig. 5). The gating mechanism we have observed with E108 has been determined as a function of the ionization of E90 in channelrhodopsin with Fourier transform infrared experiments and MD simulations (60). To the best of our knowledge, this is the first time that such an effect has been elucidated for E108 in PR.

In terms of the overall photocycle of PR, our observations bring support to the notion that PR has both similar and unique characteristics among microbial retinal proteins. Proton release in bR occurs through the utilization of two glutamic acids that act as a proton "diode" (20,61), but there is no corresponding set of residues in PR. In addition, proton release in bR occurs in the $L \rightarrow M$ transition, whereas in PR, it occurs during the last step of the photocycle (10). Our previous simulations showed that photoisomerization of retinal proceeding into the K state was sufficient to allow an influx of water into the periplasmic half channel of BPR, aided by a hydrogenbonded network centered around R94 and three tyrosine residues (31). Given the fact that the majority of conformational change that takes place in the photocycle of PR and bR occurs in the cytoplasmic half of the protein (14), our previous and current results are not surprising. However, the proton transfer we have focused on in this study (i.e., E108 to the Schiff base) that is characteristic of the $M \rightarrow N$ transition does not have a conserved set of residues in PRs. Several classes of proteobacteria with retinal-based proton pumps utilize nonacidic residues as

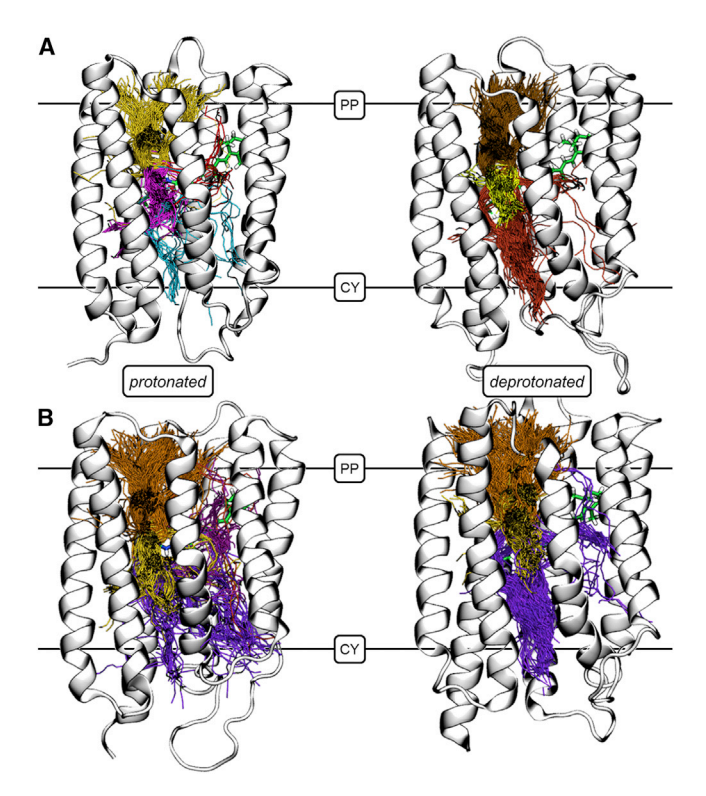


FIGURE 5 Available pathways for diffusion of water change as a function of protonation state of E108 and photoactivation of PR. (A) CAVER 3.0 was used to identify tunnels large enough to accommodate diffusion of water from outside PR to the retinal-binding pocket in the dark state. Significantly more water-accessible pathways exist in the cytoplasmic half channel of PR when E108 is deprotonated. Same-colored tunnels represent pathways from a particular cluster. Protonated E108 is located on the left, and deprotonated E108 is located on the right; sticks indicate the retinal. (B) Water-accessible tunnels in PR in the K state, identified with CAVER. Although the greatest number of tunnels are present when E108 is deprotonated, an increase in the number of tunnels is also observed for simulations when E108 is protonated. Coloring and representations are the same as in (A). CY, cytoplasmic; PP, periplasmic. To see this figure in color, go online.

a proton donor, most notably E. sibiricum PR, which uses a lysine (4), and Pseudomonas putida and Pantoea ananatis PRs, which use a glycine (30). This may be an indication that the gating mechanism we have observed in our simulations is a simpler route to hydration of the cytoplasmic half channel of PR that allows for mutations of the proton donor mentioned above while still retaining function.

Deprotonation of the proton donor perturbs the retinal-binding pocket in PR

All retinal proteins require a coordinated hydrogenbonded network within the retinal-binding pocket to stabilize the PSB in the dark state (Fig. 1). In bR, the closest homolog to PR, this network is formed by a pentameric arrangement of three water molecules with the D85 and D212 counterions (12). The crystal structure of BPR does not have a high enough resolution to identify any waters within the binding pocket (32), but the arrangement of the PSB and counterions is very similar to the retinal-binding pocket of bR in the dark state. We observe that after diffusion of water into the interior of PR, a stable pentameric arrangement of waters forms, consistent with other microbial proton pumps (62,63) (Fig. 6 A). In addition, the protonation state of E108 does not perturb the formation of the pentameric water cluster. Upon all-trans to 13-cis isomerization of retinal to generate the K photointermediate, the hydrogen of the PSB rotates away from the aspartate counterions and is no longer available to form hydrogen bonds with the water cluster. The behavior of the retinal polyene chain after isomerization is consistent with the slight out-of-plane rotation around the C14–C15 bond that was recently observed with solid-state NMR in the dark- to K-state photoactivation of GPR (64) (Table 2). This leads to a subsequent shift in the waters and counterions; one water molecule remains to coordinate with D97 and D227, but the side chains of the counterions now form direct hydrogen bonds with R94 (Fig. 6 B). This rearrangement within the retinal-binding pocket is the initial event that leads to an influx of waters from the periplasmic space, as shown from our previous study of PR (31).

In particular, of the two aspartic acid residues in the binding pocket (D97 and D227), D227 is the only one that directly forms a hydrogen bond with the PSB (Table 3). The closer interaction of D227 with the PSB compared to D97 is structurally consistent with the x-ray structure of BPR (32). In addition, this stable interaction under dynamic conditions helps validate earlier experimental investigations of the structure-function relationship of PR. One of the first studies to examine the PR photocycle with a D227N point mutant determined that D227 was responsible for selectivity of the retinal photoisomerization (predominantly 13-cis (65)). A more recent pump-probe and flash photolysis study showed that D227 is able to modulate the pK_a of the Schiff base, partially contributing to the abnormally high pK_a of the proton acceptor (\sim 7.1–7.6) with respect to that of bR (2.6) (66). We observe this direct interaction only in the dark state; after isomerization of retinal, the PSB rotates away from D97 to D227 as mentioned above (Figs. S8-S11). Deprotonation of E108 does not have any significant effect on this arrangement.

The residue at position 105 is the major determinant in the difference of spectral absorption between green and blue variants of PR: in BPR, it is a glutamine, whereas in GPR, it is a leucine. The glutamine residue in BPR is able to alter the electrostatic environment of the Schiff base. Earlier quantum mechanical calculations on a homology model of BPR in the dark state suggested that Q105 specifically influences the electronic environment around H15 of the retinal polyene chain through the formation of a hydrogen bond (67), and subsequent Fourier transform

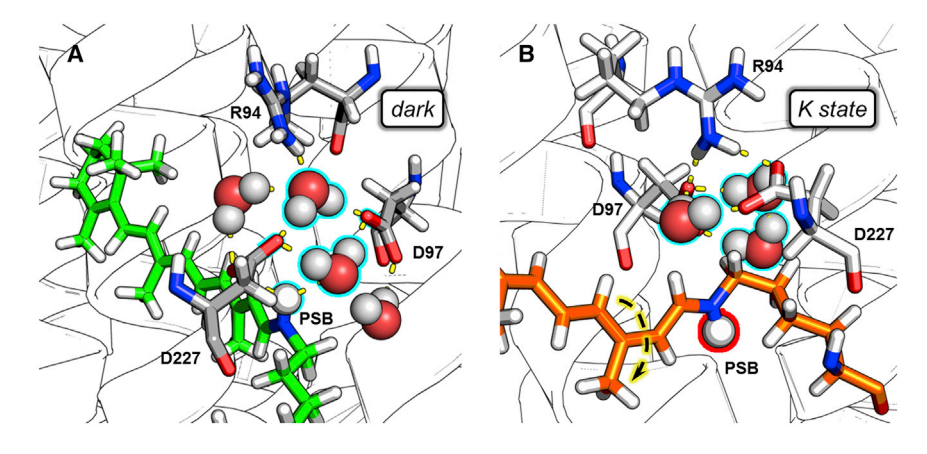


FIGURE 6 Pentameric water cluster is disrupted upon photoactivation of PR. (A) A snapshot of the retinal-binding pocket of PR with protonated E108 in the dark state. Sticks indicate the retinal (green) and important amino acid residues (gray) in the binding pocket, spheres indicate waters involved in the hydrogen-bonded network with the PSB and counterions, red indicates oxygen, white indicates hydrogen, blue indicates nitrogen, and yellow dashes indicate hydrogen bonds. The hydrogen on the PSB is rendered as a sphere. Waters and the hydrogen of the PSB are highlighted in cyan. (B) A snapshot of the retinal-binding pocket of PR in the K state is shown. After all-trans to 13-cis isomerization of retinal (dashed arrow), the PSB rotates away from the counterions, leading to a rearrangement of the water cluster. Orange sticks indicate the retinal. All other color schemes are the same as (A), with the hydrogen of the PSB highlighted in red. To see this figure in color, go online.

infrared spectroscopy studies showed that Q105 interacts with the Schiff base in both the dark and K states (34). In addition, a solid-state NMR study on a L105Q mutant of GPR showed that the presence of the glutamine side chain disrupts the conjugated π system of the polyene chain, leading to a defect in the electronic environment (68). Interestingly, we observe that the protonation state of E108 has a long-range effect on the interaction of Q105 with the retinal chromophore. In the dark state and when E108 is deprotonated, the carbonyl oxygen in the side chain of Q105 is too far to form a hydrogen bond with H14 (i.e., >5 Å; Figs. 7 A and S12). However, if E108 is protonated in the dark state, the side chain of Q105 is close enough to influence the electrostatic environment of the retinal polyene chain (\sim 5 Å; Fig. S13). Upon photoisomerization of retinal to initiate the K state, the distance between Q105 and H14 decreases to the point that a stable hydrogen bond can form, regardless of the protonation state of E108 (Fig. 7B) (69-71). This distance has a bimodal distribution for both protonation states of E108; however, when E108 is protonated, it is more than twice as likely to form a hydrogen bond (i.e., <3 Å) than when it is deprotonated.

CONCLUSION

We have studied the effect of the protonation state of the proton donor on the hydration and color tuning of BPR in

TABLE 2 Comparison of C13=C14-C15=N Dihedral of Retinal in PR

System	Dark State ^a	K State		
Protonated	$186.90^{\circ} \pm 12.46^{\circ}$	176.27° ± 12.33°		
Deprotonated	$182.03^{\circ} \pm 11.84^{\circ}$	$177.43^{\circ} \pm 11.80^{\circ}$		

^aCrystal structure of BPR (PDB: 4JQ6) has a value of 180.48°.

the early stages of photoactivation. When E108 is protonated, its side chain is oriented toward the retinal-binding pocket, preventing internal hydration of the cytoplasmic half channel. Upon deprotonation, the side chain of E108 rotates outward, facilitating the formation of a stable water channel from bulk cytoplasm to the retinal-binding pocket, in essence acting as a gating mechanism. In addition, deprotonation of E108 has distal effects on PR. In the dark state, deprotonation of E108 leads to an increase in hydration of the periplasmic half channel that is normally characteristic of the K state. In addition, deprotonation of the proton donor destabilizes interactions of the color-tuning switch, Q105, with the retinal polyene chain. Although a comprehensive picture of the proton transfers that occur during the photocycle of PR remains to be fully elucidated, our study highlights the ability of MD simulations to aid in characterizing subtle details that lead to differences in retinal proteins that act as proton pumps.

TABLE 3 Changes in Key Hydrogen-Bonding Networks in PR

System	Intermediate	PSB to D97 ^a		PSB to D227		ASP to Water ^b
		$O_{\delta 1}$	$O_{\delta 2}$	$O_{\delta 1}$	$O_{\delta 2}$	
Protonated	Dark state	0	0.1	11.9	22.3	1.3
	K state	0	0	0	0	0.3
Deprotonated	Dark state	0.2	0.1	25.1	16.3	0.7
	K state	0	0	0	0	0.7

^aAverage occupancy (in percent) of hydrogen bonds between N atom of retinal Schiff base and side-chain oxygen atoms of neighboring aspartic acids. D227 is the only counterion that is close enough to the Schiff base to directly form hydrogen bonds. However, isomerization of retinal effectively abolishes these direct interactions. D227 is believed to influence isomerization of retinal (65). This effect might be due to proximity of D227 to the retinal Schiff base.

^bAverage occupancy (in percent) of hydrogen bonds between aspartic acid residues in retinal pocket with water molecules.

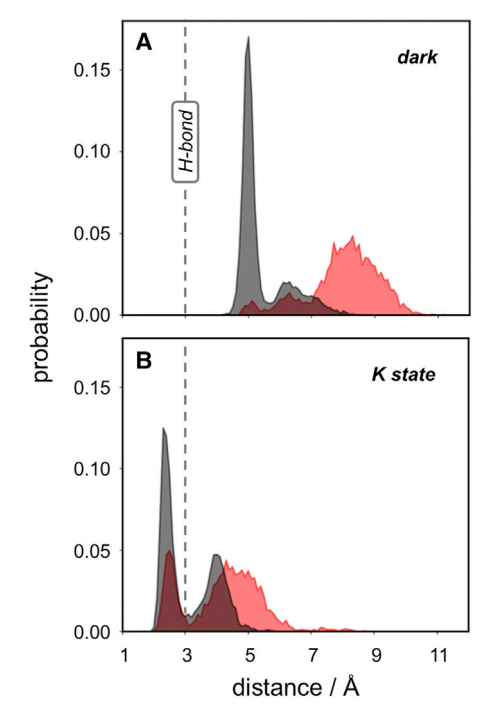


FIGURE 7 Deprotonation of E108 destabilizes interactions of Q105 with retinal. (A) Normalized distance histograms of the carbonyl oxygen of the side chain of Q105 with H14 of retinal in the dark state with E108 either protonated (black) or deprotonated (red). A clear dependence exists in the interaction of Q105 with retinal based on the protonation state of E108. Deprotonation of E108 (and subsequent hydration of the cytoplasmic interior) leads to rearrangement of the retinal-binding pocket in the vicinity of Q105. Kandori et al. hypothesized that the color-tuning mechanism of PR is based on spatial effects of residue 105 interacting with retinal and that internal hydration could play a role in stabilizing interactions with retinal (72). (B) Normalized distance histograms of the carbonyl oxygen of the side chain of Q105 with H14 of retinal in the K state with E108 either protonated (black) or deprotonated (red). Similar to the dark state, Q105 and retinal tend to be more separated when E108 is deprotonated. The all-trans to 13-cis isomerization of retinal positions Q105 significantly closer to H14. To see this figure in color, go online.

SUPPORTING MATERIAL

Fifteen figures and three tables are available at http://www.biophysj.org/ biophysj/supplemental/S0006-3495(18)30982-2.

AUTHOR CONTRIBUTIONS

S.F. and B.M. designed the research. S.F., J.F., and B.M. carried out all the simulations and analyzed the data. S.F., J.F., and B.M. wrote the article.

ACKNOWLEDGMENTS

This work was supported by West Virginia University (B.M.), the West Virginia University Nanotechnology Sensing Advances in Field and Environment program NSF EPS-1003907 (J.F.), and National Science Foundation MCB-1714888 (S.F. and B.M.). Computational time was provided through West Virginia University's Research Computing and Extreme Science and Engineering Discovery Environment (XSEDE) allocation no. TG-MCB130040.

REFERENCES

- 1. Béjà, O., L. Aravind, ..., E. F. DeLong. 2000. Bacterial rhodopsin: evidence for a new type of phototrophy in the sea. Science. 289:1902-1906.
- 2. Béjà, O., E. N. Spudich, ..., E. F. DeLong. 2001. Proteorhodopsin phototrophy in the ocean. Nature. 411:786-789.
- 3. Atamna-Ismaeel, N., G. Sabehi, ..., O. Beja. 2008. Widespread distribution of proteorhodopsins in freshwater and brackish ecosystems. ISME J. 2:656-662.
- 4. Petrovskaya, L. E., E. P. Lukashev, ..., M. P. Kirpichnikov. 2010. Predicted bacteriorhodopsin from Exiguobacterium sibiricum is a functional proton pump. FEBS Lett. 584:4193-4196.
- 5. Yutin, N., and E. V. Koonin. 2012. Proteorhodopsin genes in giant viruses. Biol. Direct. 7:34.
- 6. Slamovits, C. H., N. Okamoto, ..., P. J. Keeling. 2011. A bacterial proteorhodopsin proton pump in marine eukaryotes. Nat. Commun. 2:183.
- 7. Gómez-Consarnau, L., J. M. González, ..., J. A. Fuhrman. 2016. Proteorhodopsin light-enhanced growth linked to vitamin-B1 acquisition in marine Flavobacteria. ISME J. 10:1102-1112.
- 8. Marchetti, A., D. Catlett, ..., N. Cassar. 2015. Marine diatom proteorhodopsins and their potential role in coping with low iron availability. ISME J. 9:2745-2748.
- 9. Walter, J. M., D. Greenfield, ..., J. Liphardt. 2007. Light-powering Escherichia coli with proteorhodopsin. Proc. Natl. Acad. Sci. USA. 104:2408-2412.
- 10. Dioumaev, A. K., L. S. Brown, ..., J. K. Lanyi. 2002. Proton transfers in the photochemical reaction cycle of proteorhodopsin. *Biochemistry*. 41:5348-5358.
- 11. Váró, G., L. S. Brown, ..., J. K. Lanyi. 2003. Characterization of the photochemical reaction cycle of proteorhodopsin. Biophys. J. 84:1202-1207.
- 12. Luecke, H., B. Schobert, ..., J. K. Lanyi. 1999. Structure of bacteriorhodopsin at 1.55 Å resolution. J. Mol. Biol. 291:899–911.
- 13. Facciotti, M. T., S. Rouhani, ..., R. M. Glaeser. 2001. Structure of an early intermediate in the M-state phase of the bacteriorhodopsin photocycle. Biophys. J. 81:3442-3455.
- 14. Andersson, M., E. Malmerberg, ..., R. Neutze. 2009. Structural dynamics of light-driven proton pumps. Structure. 17:1265–1275.
- 15. Mehler, M., F. Scholz, ..., C. Glaubitz. 2013. The EF loop in green proteorhodopsin affects conformation and photocycle dynamics. *Biophys*. J. 105:385-397.
- 16. Ranaghan, M. J., S. Shima, ..., R. R. Birge. 2010. Photochemical and thermal stability of green and blue proteorhodopsins: implications for protein-based bioelectronic devices. J. Phys. Chem. B. 114:14064-
- 17. Hempelmann, F., S. Hölper, ..., C. Glaubitz. 2011. His75-Asp97 cluster in green proteorhodopsin. J. Am. Chem. Soc. 133:4645–4654.
- 18. Balashov, S. P., E. S. Imasheva, ..., T. G. Ebrey. 1996. Titration of aspartate-85 in bacteriorhodopsin: what it says about chromophore isomerization and proton release. Biophys. J. 70:473-481.
- 19. Friedrich, T., S. Geibel, ..., E. Bamberg. 2002. Proteorhodopsin is a light-driven proton pump with variable vectoriality. J. Mol. Biol. 321:821-838.
- 20. Spassov, V. Z., H. Luecke, ..., D. Bashford. 2001. pK(a) calculations suggest storage of an excess proton in a hydrogen-bonded water network in bacteriorhodopsin. J. Mol. Biol. 312:203-219.
- 21. Wang, W. W., O. A. Sineshchekov, ..., J. L. Spudich. 2003. Spectroscopic and photochemical characterization of a deep ocean proteorhodopsin. J. Biol. Chem. 278:33985-33991.
- 22. Freier, E., S. Wolf, and K. Gerwert. 2011. Proton transfer via a transient linear water-molecule chain in a membrane protein. Proc. Natl. Acad. Sci. USA. 108:11435-11439.

- 23. Váró, G., and J. K. Lanyi. 1991. Distortions in the photocycle of bacteriorhodopsin at moderate dehydration. Biophys. J. 59:313-322.
- 24. Cao, Y., G. Váró, ..., J. K. Lanyi. 1991. Water is required for proton transfer from aspartate-96 to the bacteriorhodopsin Schiff base. Biochemistry. 30:10972-10979.
- 25. Brown, L. S., G. Váró, ..., J. K. Lanyi. 1995. Functional significance of a protein conformation change at the cytoplasmic end of helix F during the bacteriorhodopsin photocycle. Biophys. J. 69:2103-2111.
- 26. Wang, T., A. O. Sessions, ..., M. T. Facciotti. 2013. Deprotonation of D96 in bacteriorhodopsin opens the proton uptake pathway. Structure. 21:290-297.
- 27. Wang, T., C. Oppawsky, ..., M. T. Facciotti. 2014. Stable closure of the cytoplasmic half-channel is required for efficient proton transport at physiological membrane potentials in the bacteriorhodopsin catalytic cycle. Biochemistry. 53:2380-2390.
- 28. Lorenz-Fonfria, V. A., M. Saita, ..., J. Heberle. 2017. pH-sensitive vibrational probe reveals a cytoplasmic protonated cluster in bacteriorhodopsin. Proc. Natl. Acad. Sci. USA. 114:E10909-E10918.
- 29. Gushchin, I., P. Chervakov, ..., V. Gordeliy. 2013. Structural insights into the proton pumping by unusual proteorhodopsin from nonmarine bacteria. Proc. Natl. Acad. Sci. USA. 110:12631-12636.
- 30. Harris, A., M. Ljumovic, ..., L. S. Brown. 2015. A new group of eubacterial light-driven retinal-binding proton pumps with an unusual cytoplasmic proton donor. Biochim. Biophys. Acta. 1847:1518–1529.
- 31. Feng, J., and B. Mertz. 2015. Proteorhodopsin activation is modulated by dynamic changes in internal hydration. Biochemistry. 54:7132-7141.
- 32. Ran, T., G. Ozorowski, ..., H. Luecke. 2013. Cross-protomer interaction with the photoactive site in oligomeric proteorhodopsin complexes. Acta Crystallogr. D Biol. Crystallogr. 69:1965-1980.
- 33. Reckel, S., D. Gottstein, ..., V. Dötsch. 2011. Solution NMR structure of proteorhodopsin. Angew. Chem. Int. Engl. 50:11942-11946.
- 34. Amsden, J. J., J. M. Kralj, ..., K. J. Rothschild. 2008. Different structural changes occur in blue- and green-proteorhodopsins during the primary photoreaction. *Biochemistry*. 47:11490–11498.
- 35. Dowhan, W. 1997. Molecular basis for membrane phospholipid diversity: why are there so many lipids? Annu. Rev. Biochem. 66:199–232.
- 36. Jo, S., T. Kim, and W. Im. 2007. Automated builder and database of protein/membrane complexes for molecular dynamics simulations. PLoS One. 2:e880.
- 37. Jo, S., J. B. Lim, ..., W. Im. 2009. CHARMM-GUI Membrane builder for mixed bilayers and its application to yeast membranes. Biophys. J. 97:50-58.
- 38. Jo, S., T. Kim, ..., W. Im. 2008. CHARMM-GUI: a web-based graphical user interface for CHARMM. J. Comput. Chem. 29:1859-1865.
- 39. Lee, J., X. Cheng, ..., W. Im. 2016. CHARMM-GUI input generator for NAMD, GROMACS, AMBER, OpenMM, and CHARMM/OpenMM simulations using the CHARMM36 additive force field. J. Chem. Theory Comput. 12:405-413.
- 40. Phillips, J. C., R. Braun, ..., K. Schulten. 2005. Scalable molecular dynamics with NAMD. J. Comput. Chem. 26:1781-1802.
- 41. Vanommeslaeghe, K., E. Hatcher, ..., A. D. Mackerell, Jr. 2010. CHARMM general force field: a force field for drug-like molecules compatible with the CHARMM all-atom additive biological force fields. J. Comput. Chem. 31:671-690.
- 42. Zhu, S., M. F. Brown, and S. E. Feller. 2013. Retinal conformation governs pKa of protonated Schiff base in rhodopsin activation. J. Am. Chem. Soc. 135:9391-9398.
- 43. Mertz, B., M. Lu, ..., S. E. Feller. 2011. Steric and electronic influences on the torsional energy landscape of retinal. Biophys. J. 101:L17-L19.
- 44. Crowley, M. F., M. J. Williamson, and R. C. Walker. 2009. CHAMBER: comprehensive support for CHARMM force fields within the AMBER software. Int. J. Quantum Chem. 109:3767-3772.
- 45. Salomon-Ferrer, R., A. W. Götz, ..., R. C. Walker. 2013. Routine microsecond molecular dynamics simulations with AMBER on

- GPUs. 2. Explicit solvent particle mesh Ewald. J. Chem. Theory Comput. 9:3878-3888.
- 46. Case, D. A., R. M. Betz, ..., P. A. Kollman. 2016. AMBER 2016. University of California, San Francisco, CA.
- 47. Martínez-Mayorga, K., M. C. Pitman, ..., M. F. Brown. 2006. Retinal counterion switch mechanism in vision evaluated by molecular simulations. J. Am. Chem. Soc. 128:16502-16503.
- 48. Kirkwood, J. G. 1936. Statistical mechanics of liquid solutions. Chem. Rev. 19:275-307.
- 49. Straatsma, T. P., and J. A. McCammon. 1991. Multiconfiguration thermodynamic integration. J. Chem. Phys. 95:1175-1188.
- 50. Humphrey, W., A. Dalke, and K. Schulten. 1996. VMD: visual molecular dynamics. J. Mol. Graph. 14:33-38, 27-28.
- 51. Schrödinger, LLC.. 2010. The PyMOL Molecular Graphics System, Version 1.3r1. Schrödinger, LLC, New York.
- 52. Michaud-Agrawal, N., E. J. Denning, ..., O. Beckstein. 2011. MDAnalysis: a toolkit for the analysis of molecular dynamics simulations. J. Comput. Chem. 32:2319-2327.
- 53. Pavelka, A., E. Sebestova, ..., J. Damborsky. 2016. CAVER: algorithms for analyzing dynamics of tunnels in macromolecules. IEEE/ ACM Trans. Comput. Biol. Bioinformatics. 13:505-517.
- 54. Chovancova, E., A. Pavelka, ..., J. Damborsky. 2012. CAVER 3.0: a tool for the analysis of transport pathways in dynamic protein structures. PLoS Comput. Biol. 8:e1002708.
- 55. LeVine, M. V., and H. Weinstein. 2014. NbIT-a new information theory-based analysis of allosteric mechanisms reveals residues that underlie function in the leucine transporter LeuT. PLoS Comput. Biol. 10:e1003603.
- 56. LeVine, M. V., J. M. Perez-Aguilar, and H. Weinstein. 2014. N-body information theory (NbIT) analysis of rigid-body dynamics in intracellular loop 2 of the 5-HT2A receptor. arXiv, arXiv:1406.4730.
- 57. Schobert, B., L. S. Brown, and J. K. Lanyi. 2003. Crystallographic structures of the M and N intermediates of bacteriorhodopsin: assembly of a hydrogen-bonded chain of water molecules between Asp-96 and the retinal Schiff base. J. Mol. Biol. 330:553–570.
- 58. Arnis, S., K. Fahmy, ..., T. P. Sakmar. 1994. A conserved carboxylic acid group mediates light-dependent proton uptake and signaling by rhodopsin. J. Biol. Chem. 269:23879-23881.
- 59. Vogel, R., M. Mahalingam, ..., T. P. Sakmar. 2008. Functional role of the "ionic lock"-an interhelical hydrogen-bond network in family A heptahelical receptors. J. Mol. Biol. 380:648-655.
- 60. Eisenhauer, K., J. Kuhne, ..., K. Gerwert. 2012. In channelrhodopsin-2 Glu-90 is crucial for ion selectivity and is deprotonated during the photocycle. J. Biol. Chem. 287:6904-6911.
- 61. Zscherp, C., R. Schlesinger, ..., J. Heberle. 1999. In situ determination of transient pKa changes of internal amino acids of bacteriorhodopsin by using time-resolved attenuated total reflection Fourier-transform infrared spectroscopy. Proc. Natl. Acad. Sci. USA. 96:5498-5503.
- 62. Kandori, H., Y. Yamazaki, ..., A. Maeda. 1995. Water-mediated proton transfer in proteins: an FTIR study of bacteriorhodopsin. J. Am. Chem. Soc. 117:2118-2119.
- 63. Hatanaka, M., H. Kandori, and A. Maeda. 1997. Localization and orientation of functional water molecules in bacteriorhodopsin as revealed by polarized Fourier transform infrared spectroscopy. Biophys. J. 73:1001-1006.
- 64. Mehler, M., C. E. Eckert, ..., C. Glaubitz. 2017. Chromophore distortions in photointermediates of proteorhodopsin visualized by dynamic nuclear polarization-enhanced solid-state NMR. J. Am. Chem. Soc. 139:16143-16153.
- 65. Imasheva, E. S., S. P. Balashov, ..., J. K. Lanyi. 2004. Selectivity of retinal photoisomerization in proteorhodopsin is controlled by aspartic acid 227. Biochemistry. 43:1648-1655.
- 66. Herz, J., M. K. Verhoefen, ..., J. Wachtveitl. 2012. Critical role of Asp227 in the photocycle of proteorhodopsin. Biochemistry. 51:5589-5600.

Faramarzi et al.

- 67. Hillebrecht, J. R., J. Galan, ..., R. R. Birge. 2006. Structure, function, and wavelength selection in blue-absorbing proteorhodopsin. Biochemistry. 45:1579–1590.
- 68. Mao, J., N. N. Do, ..., C. Glaubitz. 2014. Structural basis of the greenblue color switching in proteorhodopsin as determined by NMR spectroscopy. J. Am. Chem. Soc. 136:17578-17590.
- 69. Sutor, D. J. 1962. The C-H... O hydrogen bond in crystals. Nature. 195:68-69.
- 70. Desiraju, G. R. 1996. The C-h \cdots o hydrogen bond: structural implications and supramolecular design. Acc. Chem. Res. 29:441-449.
- 71. Gu, Y., T. Kar, and S. Scheiner. 1999. Fundamental Properties of the CH · · · O interaction: is it a true hydrogen bond? J. Am. Chem. Soc. 121:9411-9422.
- 72. Ozaki, Y., T. Kawashima, ..., H. Kandori. 2014. A color-determining amino acid residue of proteorhodopsin. Biochemistry. 53:6032-6040.